


SCIENTIFIC REPORTS



OPEN

3D hierarchical assembly of ultrathin MnO₂ nanoflakes on silicon nanowires for high performance micro-supercapacitors in Li- doped ionic liquid

Received: 03 December 2014

Accepted: 16 March 2015

Published: 18 May 2015

Deepak P. Dubal¹, David Aradilla^{2,3,4}, Gérard Bidan⁵, Pascal Gentile^{6,7}, Thomas J.S. Schubert⁸, Jan Wimberg⁸, Saïd Sadki^{2,3,4} & Pedro Gomez-Romero^{1,9}

Building of hierarchical core-shell hetero-structures is currently the subject of intensive research in the electrochemical field owing to its potential for making improved electrodes for high-performance micro-supercapacitors. Here we report a novel architecture design of hierarchical MnO₂@silicon nanowires (MnO₂@SiNWs) hetero-structures directly supported onto silicon wafer coupled with Li-ion doped 1-Methyl-1-propylpyrrolidinium bis(trifluoromethylsulfonyl)imide (PMPYrrBTA) ionic liquids as electrolyte for micro-supercapacitors. A unique 3D mesoporous MnO₂@SiNWs in Li-ion doped IL electrolyte can be cycled reversibly across a voltage of 2.2V and exhibits a high areal capacitance of 13 mFcm⁻². The high conductivity of the SiNWs arrays combined with the large surface area of ultrathin MnO₂ nanoflakes are responsible for the remarkable performance of these MnO₂@SiNWs hetero-structures which exhibit high energy density and excellent cycling stability. This combination of hybrid electrode and hybrid electrolyte opens up a novel avenue to design electrode materials for high-performance micro-supercapacitors.

Micro-supercapacitors are miniaturized electrochemical energy storage devices, recently developed, which can offer power densities several orders of magnitude larger than those of conventional batteries and supercapacitors due to their short ion diffusion lengths¹⁻⁴. Remarkably, such microdevices can be directly integrated into other miniaturized electronic devices such as sensors-actuators or energy-harvesting microsystems providing excellent nano-/micro-scale peak power⁵⁻⁷. Recently, great efforts have been devoted to increase the energy and power densities of micro-supercapacitors via the fabrication of nano-structured electroactive materials such as carbide-derived carbon², carbon onions³ and the development of thin-film manufacture technologies for example electrochemical polymerization¹, inkjet printing⁸, and layer-by-layer assembly⁹. In spite of such great advancements, the development of high performance micro-supercapacitors is still a challenge.

The last few years have witnessed a burst of reports on the use of silicon nanowires (SiNW) as electrode materials for micro-supercapacitors due to their fascinating capacitive properties. These include

¹Catalan Institute of Nanoscience and Nanotechnology, CIN2, ICN2 (CSIC-ICN), Campus UAB E-08193, Bellaterra, Barcelona. ²Univ. Grenoble Alpes, INAC-SPRAM, F-38000 Grenoble, France. ³CNRS, SPRAM, F-38000 Grenoble, France. ⁴CEA, INAC-SPRAM, F-38000 Grenoble, France. ⁵Univ. Grenoble Alpes, INAC-DIR, F-38000 Grenoble, France, CEA, INAC-DIR F-38000, Grenoble, France. ⁶Univ. Grenoble Alpes, INAC-SP2M-SiNaPs, F-38000 Grenoble, France. ⁷CEA, INAC-SP2M-SiNaPs, F-38000 Grenoble, France. ⁸IOLITEC Ionic Liquids Technologies GmbH, Salzstrasse 184, 74076, Heilbronn, Germany. ⁹Consejo Superior de Investigaciones Científicas (CSIC), Spain. Correspondence and requests for materials should be addressed to P.G.-R. (email: pedro.gomez@cin2.es)

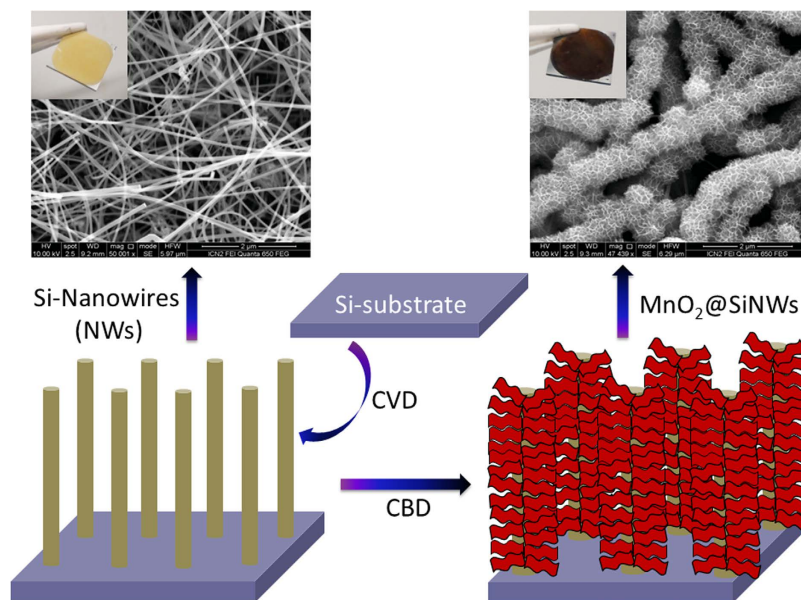


Figure 1. Schematic illustration of steps involved in the fabrication of MnO_2 @SiNWs core-shell hetero-structure along with SEM images and digital photographs of SiNWs and MnO_2 @SiNWs.

plain silicon nanowires (SiNWs)¹⁰, as well as doped SiNWs^{11,12}, silicon carbide nanowires¹³, porous silicon coated with gold^{14,15}. Moreover, in order to improve the capacitive properties of SiNWs, the development of core-shell nanostructures has been intensively investigated very recently, including NiO/SiNWs^{16,17}, poly(3,4-ethylenedioxythiophene) (PEDOT)/SiNW¹⁸ etc. However, due to the intrinsically poor electrical conductivity of metal oxides and the short diffusion distance of electrolytes into pseudocapacitor electrodes, only the surface of electroactive materials can effectively contribute to the total capacitance while the large portion of material underneath the surface could hardly participate in the electrochemical charge storage process, leading to values of areal specific capacitance (ASC) lower than expected. Therefore, it is still a great challenge to boost the electrochemical utilization and ASC of pseudocapacitive materials by rationally designing electrodes with novel microstructures. An emerging attractive concept is to directly grow smart integrated array architectures with the combination of two types of materials and/or nanostructures on conducting substrates as binder-free electrodes for micro-supercapacitors. In this way, many advantages such as multiple accessible electroactive sites, short ion transport pathways, superior electron collection efficiency, and even fascinating synergetic properties are simultaneously achieved to deliver high ASC, sustained cycle life and rate performance.

The overall performance of a supercapacitor depends not only on the electrode materials employed but also on the electrolytes used. Ionic liquids are more expensive than aqueous electrolytes but their relatively superior properties such as high thermal stability, large potential window etc. makes them more promising in supercapacitors. MnO_2 films with common ionic liquid (IL) electrolyte-based supercapacitors have been investigated with an electrochemical quartz-crystal microbalance (EQCM), X-ray photoemission spectroscopy (XPS)¹⁹ and *in situ* X-ray absorption spectroscopy (XAS)²⁰. It is reported that the most common cations, such as n-butyl-n-methylpyrrolidinium⁺, 1-ethyl-3-methylimidazolium⁺ and 1-butyl-3-methyl-imidazolium⁺, adsorb only onto the electrode surface of the MnO_2 films and do not penetrate into tunnels within the $[\text{MnO}_6]$ octahedral framework. Thus, a low percentage of Mn in the structure undergoes redox processes with ionic liquid (IL) electrolytes, indicating that ion insertion is correspondingly low. Thus, novel ionic liquid with appropriate cations that enable compensation of the redox reaction during charge and discharge cycles are crucial to improve the capacity performance of MnO_2 films.

Based on the above considerations, we have fabricated and patented [ref] a unique design of hierarchical MnO_2 @SiNWs core-shell hetero-structure coupled with a novel Li-ion doped ionic liquid as electrolyte, which is based on LiClO_4 and 1-Methyl-1-propylpyrrolidinium bis(trifluoromethylsulfonyl)imide (PMPyrrBTA) for high-performance micro-supercapacitors. In this case the slim SiNWs are the “core” and ultrathin MnO_2 nanoflakes the “shell” layer. Initially, SiNWs were grown on silicon wafer by chemical vapor deposition (CVD) technique on which subsequent deposition of ultrathin MnO_2 nanoflakes using chemical bath deposition (CBD) method was carried out. Figure 1 shows a schematic illustration of steps involved in the fabrication of MnO_2 @SiNWs core-shell hetero-structure along with SEM and digital photographs. This MnO_2 @SiNWs device can be cycled reversibly at a high operating voltage of 2.2 V with good capacitance, energy density and excellent cycling stability in a LiClO_4 -PMPyrrBTA IL electrolyte.

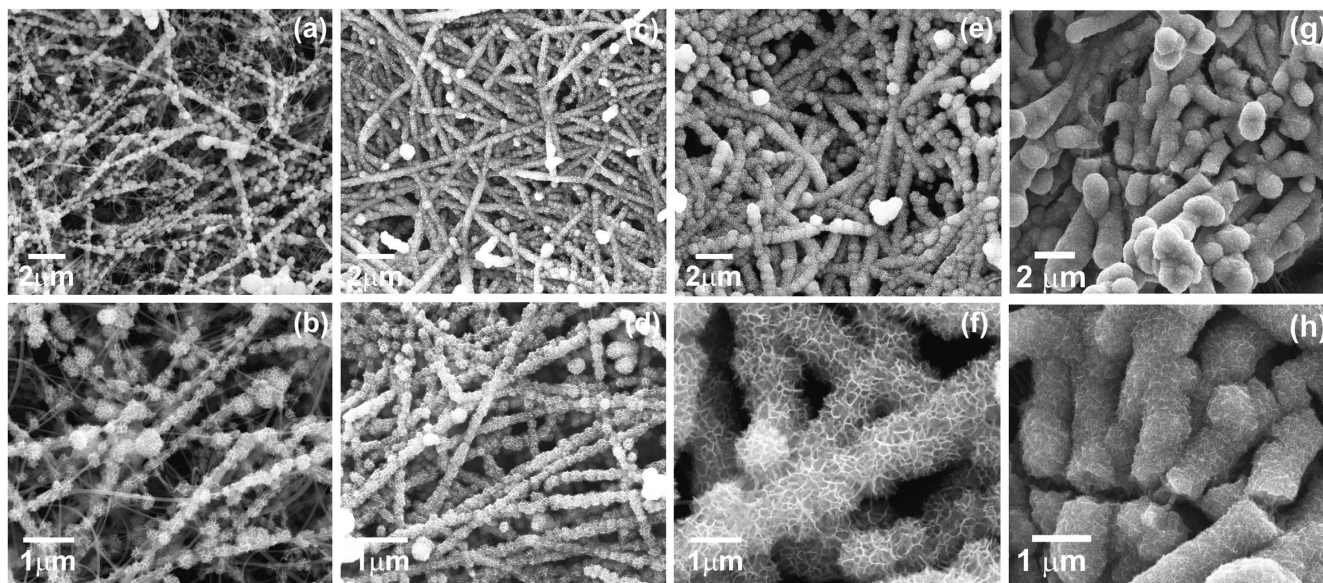


Figure 2. SEM images of the MnO₂@SiNWs hetero-structures prepared at different deposition times (a, b) 5 min, (c, d) 10 min, (e, f) 15 min and (g, h) 20 min at two different magnifications, respectively.

Results

Figure 2 presents SEM images of the MnO₂@SiNWs hetero-structures prepared for different deposition times at two different magnifications. From Fig. 2a,b, one can see that surfaces of SiNWs nanowires are partly covered by MnO₂ nanoflakes after just 5 minutes of reaction. Yet, many of the nanowires remain uncoated, which indicates an insufficient deposition time. As the reaction time increased to 10 min, almost the whole surfaces of Si nanowires are homogeneously covered by ultrathin MnO₂ nanoflakes (Fig. 2c,d). Further increase in reaction time (15 min) results in SiNWs surfaces covered by highly mesoporous MnO₂ nanoflakes (Fig. 2e,f), indicative of a sufficiently long reaction time with KMnO₄. On closer inspection, the individual hierarchical MnO₂@SiNWs hetero-structure is determined to have a much larger diameter (Fig. 2f), than the pristine Si nanowires. Finally, when the reaction time is 20 min, the resulting hetero-structure is extra thick but less porous and begins to show signs of damage. Indeed, high magnification images show some cracks on the surfaces, not observed in the structures grown during shorter times and therefore most likely due to the over-loading of MnO₂ on SiNWs (Fig. 2g,h).

Figure 3a,b shows TEM images of the MnO₂@SiNWs core-shell hetero-structure prepared in 15 min time. The surfaces of Si nanowires are uniformly covered by ultrathin nanoflakes (Fig. 3b). The surface of the nanoflake is highly transparent, suggesting very small thickness (~2–5 nm). Further analysis of the SAED pattern (inset of Fig. 3b) taken from the nanoflake edge reveals the formation of birnessite-type polycrystalline MnO₂^{21,22}. From the HRTEM image (Fig. 3c), one can clearly see the lattice fringes with an interplanar spacing of 0.69 nm for the two curling nanosheets, which is identified as the characteristic interplanar spacing of the (001) plane of birnessite-type MnO₂.

The proposed growth mechanism for MnO₂@SiNWs core-shell hetero-structure is as follows: Initially, MnO₄⁻ nuclei are produced and adsorbed on surfaces of SiNWs, and form MnO₂ nuclei upon reduction. With the increase in reaction time, the MnO₂ nuclei grow and are aggregated and transformed to nanoflakes since thermodynamically, surface energy of individual nanoflakes is high hence they start to self-aggregate (supporting information S1). At the end, the MnO₂ nanoflake is compact and totally covers the surface of Si nanowires, resulting in the formation of the hierarchical MnO₂@SiNWs core-shell hetero-structure. Such process is supported by the morphology evolution at different growth stages via tuning the reaction time. In order to determine the crystal phases present in the MnO₂@SiNWs hetero-structures, X-ray diffraction (XRD) analyses were carried out, as shown in Fig. 3d, where XRD patterns of MnO₂ grown SiNWs at different deposition times are presented. The diffraction peaks can be indexed as (001), (002), (-111) and (020) corresponding to the birnessite manganese dioxide phase (JCPDS card no. 80–1098, space group of C2/m), and confirming the expected formation of MnO₂. Figure 3e,f shows XPS spectra of the MnO₂@SiNWs, which are calibrated with reference to C1s peak at 285 eV (supporting information S3). The Mn2p XPS spectrum exhibits two major peaks at binding energies of 642.2 and 654 eV with a spin-energy separation of 11.8 eV (Fig. 3e), in agreement with other reports on MnO₂ phases²³. As reported previously²⁴, the average oxidation state of Mn in manganese oxides can be determined by the energy separation of Mn3s peaks. The MnO₂@SiNWs hybrid structures exhibit an energy separation of 4.85 eV for the Mn3s doublet (Fig. 3f), indicating that Mn in the hetero-structure has an oxidation state of Mn(IV).

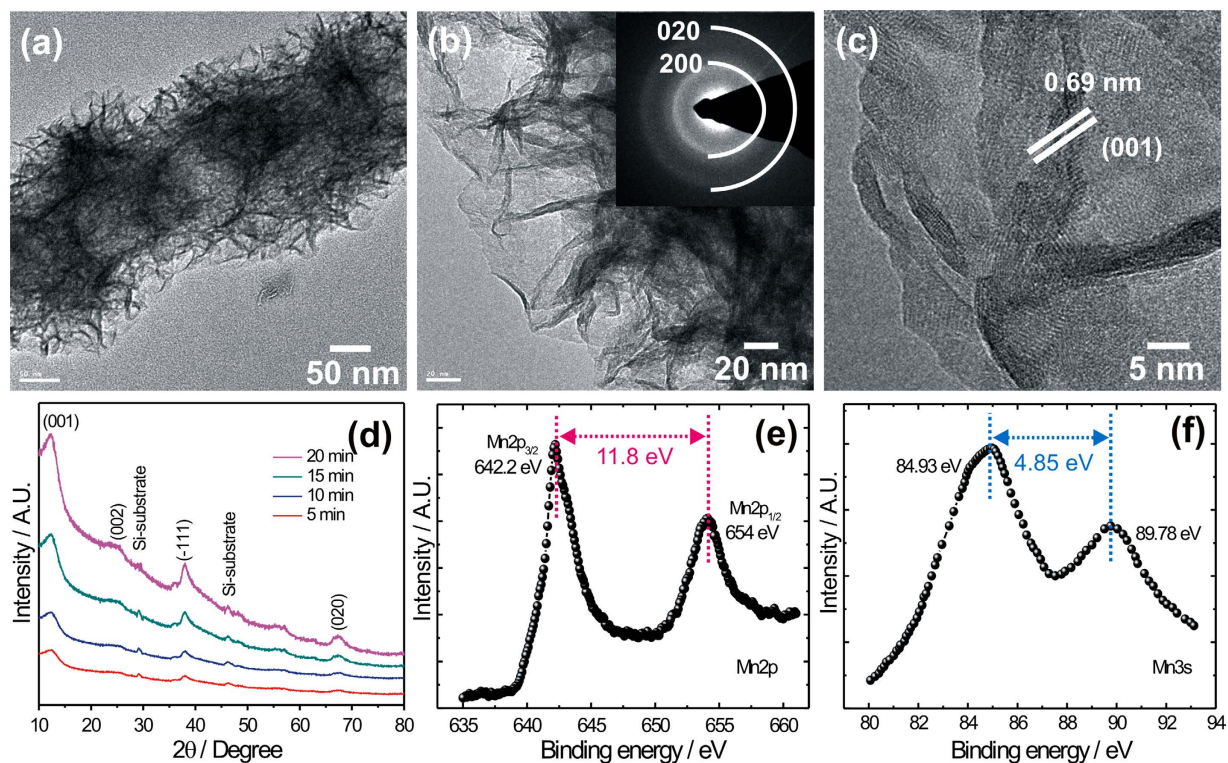


Figure 3. (a–c) TEM and HRTEM images of the MnO₂@SiNWs core-shell hetero-structure prepared at the time interval of 15 min, SAED pattern (inset of Fig. 3b) taken from the nanoflake edge. Figure 3 (d) XRD patterns of MnO₂ grown SiNWs at different deposition times. Figure 3 (e,f) core level XPS of Mn2p and Mn3s spectra for MnO₂@SiNWs hybrid materials, respectively.

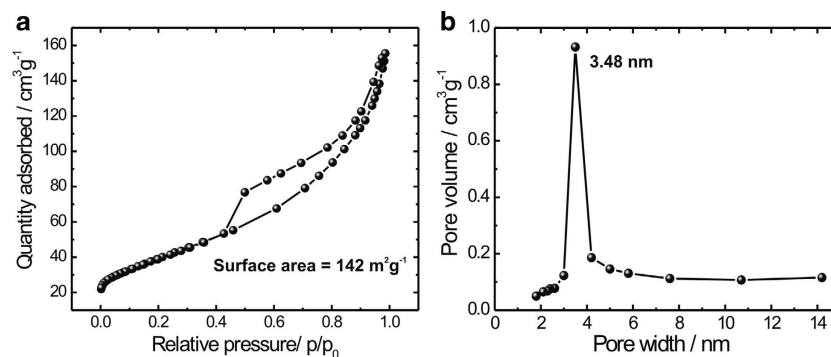


Figure 4. (a) Nitrogen adsorption/desorption isotherm of MnO₂@SiNWs sample (synthesized at 15 min time interval) (b) BJH pore size distribution plot of MnO₂@SiNWs.

To further investigate the surface properties of hierarchical MnO₂@SiNWs core-shell hetero-structures, we performed Brunauer-Emmett-Teller (BET) analysis on adsorption isotherms shown in Fig. 4(a). The MnO₂@SiNWs hybrid structure shows a typical IV-type isotherm with hysteresis loop in a relative pressure (p/p_0) range of 0.4–1.0, implying the formation of slit-like pores, a type of porosity which can be easily understood as a result of the stacking of MnO₂ flakes. The BET surface area of the MnO₂@SiNWs core-shell hetero-structure is calculated to be 142 m² g⁻¹ which is much higher than plate-like (23–43 m² g⁻¹) or comparable to nanorods (100–150 m² g⁻¹), hollow spheres (52–108 m² g⁻¹) and urchin-like (80–119 m² g⁻¹) MnO₂ structures²⁵. Figure 4b shows the Barrett-Joyner-Halenda (BJH) pore size distribution curve with a distinct maximum centered at ~3.5 nm. This confirms the mesoporous nature of MnO₂@SiNWs hybrid structure. The mesoporosity of MnO₂@SiNWs samples results from a combination of internal space of the agglomerated nanoflakes and surface rugosity of the individual nanoflakes. Such type of hierarchical surface morphologies with high surface area and mesoporous nature can

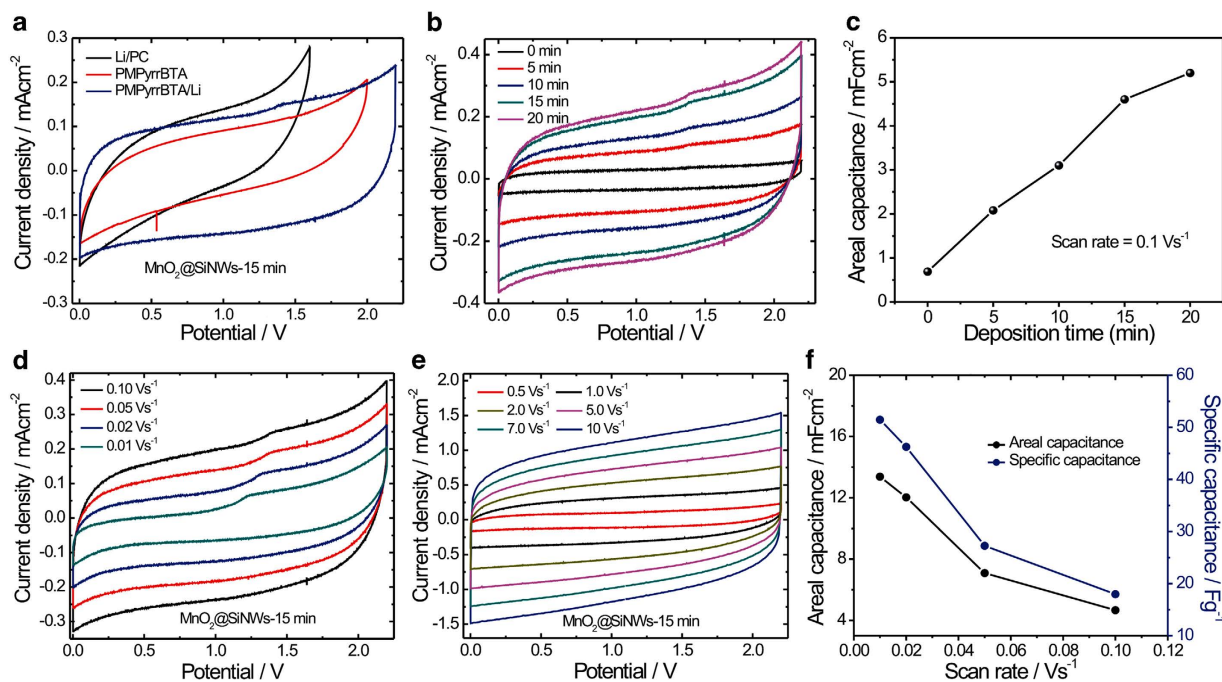


Figure 5. (a) CV curves of MnO₂@SiNWs electrodes in LiClO₄/propylene carbonate, 1-Methyl-1-propylpyrrolidinium bis(trifluoromethylsulfonyl)imide (PMPyrrBTA) and LiClO₄ doped ionic liquid electrolyte (LiClO₄-PMPyrrBTA). (b) CV curves corresponding to the different MnO₂ deposition times. (c) Variation of areal capacitance with mass loading of MnO₂ on SiNWs in Li-ion doped ionic liquid electrolyte. (d-e) CVs curves of MnO₂@SiNWs (synthesized at 15 min) at different scan rates from 0.01 Vs⁻¹ to 10 Vs⁻¹. (f) Variation of areal and specific capacitance with scan rate of MnO₂@SiNWs electrodes.

enhance electrochemical properties since large pore channels permit rapid electrolyte transport, while the small pores provide more active sites for chemical reactions^{26,27}.

To evaluate the electrochemical performance of the MnO₂@SiNWs hetero-structure, two-electrode configuration was used in the electrochemical measurements. Figure 5(a) presents the CV curves of MnO₂@SiNWs electrodes in three different electrolytes, namely i) LiClO₄/propylene carbonate, ii) 1-Methyl-1-propylpyrrolidinium bis(trifluoromethylsulfonyl)imide (PMPyrrBTA) and iii) LiClO₄ doped ionic liquid electrolyte (LiClO₄-PMPyrrBTA). Although there are no distinct redox peaks, the shape of CV curve in LiClO₄/PC electrolyte deviates from the ideal rectangle, implying that the electrode shows faradaic pseudocapacitive nature. However, in PMPyrrBTA, and even more clearly so in Li⁺-doped PMPyrrBTA, the shape of the CV curve is nearly rectangular, indicating that the MnO₂@SiNWs electrode has satisfactory capacitive behavior in these electrolytes. Furthermore, it is interesting to note that the MnO₂@SiNWs electrode in Li⁺-doped PMPyrrBTA electrolyte has a substantially larger CV area than in pure PMPyrrBTA. The rectangular CV response, which reflects the pseudocapacitive behavior, was attributed to a continuous and reversible faradaic reaction of the Mn-oxide. Thus, the addition of Li salt in ionic liquid electrolyte significantly increases the electrochemical performance of the MnO₂@SiNWs electrodes.

In order to investigate the relationship between the deposition time of MnO₂ and the performances of the devices, we have varied MnO₂ deposition time from 0 to 20 min. CV curves corresponding to the different MnO₂ deposition times were measured and are illustrated in Fig. 5(b). All the CV curves were measured at a scan rate of 100 mV/s but show obvious differences. From CV curves, it is seen that, the areal capacitance (related to the area under the CV curves) increases proportionally to deposition time up to 15 min, then gets stabilized at ca. 5.2 mFcm⁻² as deposition time reaches 20 min Fig. 5(c). We should recall that the microstructural analysis by electron microscopy indicated that the mesoporous structure of MnO₂ coating on SiNWs started to damage for deposition times longer than 15 min (see SEM micrographs in Fig. 2). Hence, we can conclude that both from a microstructural and an electrochemical point of view, 15 min is an optimal deposition time for MnO₂.

Next, in order to highlight the merits of this unique hybrid architecture, we tested the hierarchical MnO₂@SiNWs nanowires as electrodes in symmetrical supercapacitors (two-electrode configuration). For reference, CV curves of MnO₂ and SiNWs have been tested and in Li-ion doped ionic liquid electrolyte (LiClO₄-PMPyrrBTA) and shown in supporting information S4. Figure 5(d-e) shows the cyclic voltammograms (CVs) of MnO₂@SiNWs at different scan rates from 0.01 Vs⁻¹ to 10 Vs⁻¹ suggesting that the MnO₂@SiNWs devices can be operated over a wide range of scan rates. Moreover, the CV profiles of the MnO₂@SiNWs electrodes show the rectangular shape characteristic of capacitive energy storage. This

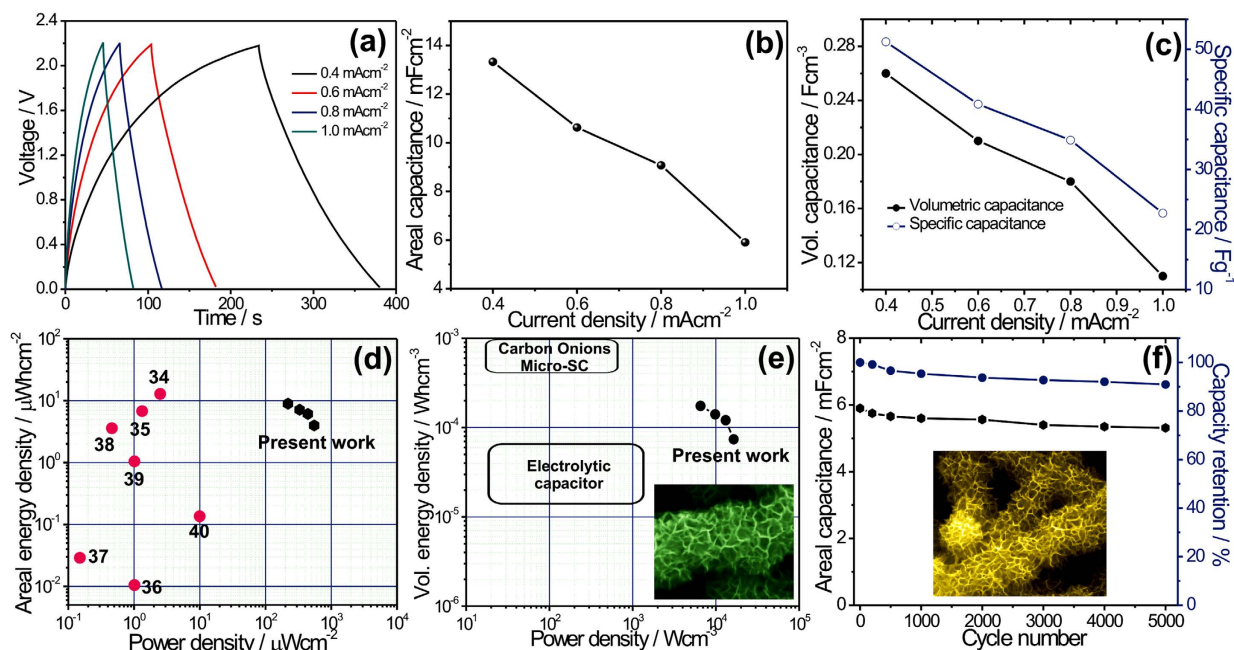


Figure 6. (a) Galvanostatic charge-discharge curves of $\text{MnO}_2@\text{SiNWs}$ hybrid in Li-ion doped ionic liquid electrolyte at various current densities. (b–c) The areal, volume and specific capacitances of the $\text{MnO}_2@\text{SiNWs}$ symmetric device measured at different current densities. (d) Plot of areal energy density versus areal power density of $\text{MnO}_2@\text{SiNWs}$ device with comparison to other reported values. (e) Plot of volumetric power and energy densities of the $\text{MnO}_2@\text{SiNWs}$ device comparing with other energy storage devices. (f) Variation of areal capacitance and capacity retention with number of cycles for 5000 cycles.

shape remains unchanged as the scan rate increases from 0.01 Vs^{-1} to 10 Vs^{-1} , demonstrating good capacitive properties and high-rate capability. Furthermore, the area integrated within the current-potential curves greatly increases for the core-shell arrays as compared with bare SiNWs. This represents a much larger capacity for the hybrid nanowires, which must be attributed to the additional pseudocapacitance provided by the superficial intercalation of Li^+ ions into the thin MnO_2 flakes that form the nanowires shell. Also, the high scan rate that $\text{MnO}_2@\text{SiNWs}$ can achieve (10 Vs^{-1}) implies an ultrahigh power density for these unique core-shell hetero-structures. Figure 5(f) shows the variation of areal and specific capacitance with scan rate for $\text{MnO}_2@\text{SiNWs}$ electrodes. The highest areal capacitance obtained for the $\text{MnO}_2@\text{SiNWs}$ electrode was 13.38 mFcm^{-2} (51.46 Fg^{-1} , for mass loading of 0.26 mgcm^{-2}) at 0.01 Vs^{-1} , which is much higher than the values obtained for the pristine SiNWs (ranging from 0.01 – 0.05 mFcm^{-2})^{11–15} and SiNWs based nanocomposites (for details see supporting information S5). The high areal capacitances we report here are also superior to those found for any of other recently reported hybrid nanostructures. For example $\text{MnO}_2/\text{onion}$ like carbon (MnO_2/OLC) (7.04 mFcm^{-2} at 0.02 mAcm^{-2})²⁸, $\text{MWCNT}/\text{MnO}_2$ (2.43 mFcm^{-2} at 0.5 mA)²⁹, CNT/MnO_2 (3.01 mFcm^{-2} at 0.002 mA)³⁰, or conducting polymer (PEDOT) coated SiNWs (9 mFcm^{-2} at 0.1 mAcm^{-2})¹⁸. Moreover, $\text{MnO}_2@\text{SiNWs}$ electrodes exhibit a good rate capability with capacity retention of 34.90% of the initial capacitance as the scan rate increases from 0.01 to 0.1 Vs^{-1} . Furthermore, it should be remarked that the $\text{MnO}_2@\text{SiNWs}$ hybrid symmetric micro-supercapacitors reported here also show better performance in terms of specific capacitance (13.9 mFcm^{-2} at 0.01 Vs^{-1}) than interdigitated on-chip micro-supercapacitors based on carbide derived carbon films (e.g. SC: 1.5 mFcm^{-2} at 0.1 Vs^{-1})³¹, or onion-like carbon based micro-supercapacitor electrodes prepared by electrophoretic deposition (e.g. SC: 1.1 mFcm^{-2} at 0.2 Vs^{-1})³².

To further investigate electrochemical performances of the $\text{MnO}_2@\text{SiNWs}$ symmetric device, we carried out galvanostatic charge-discharge cycles at various current densities (Fig. 6(a)). The charging and discharging parts of the curves are not perfectly linear which indicates a contribution from the pseudocapacitive mechanism associated to surface intercalation of Li^+ onto MnO_2 . Additionally, a very small iR drop (where i and R represent the current and resistance) for the $\text{MnO}_2@\text{SiNWs}$ electrode was observed. This small ohmic drop can be the result of a series of low-resistance connections provided by the solid connection between the silicon substrate and Si nanowires, between the nanowires and MnO_2 thin sheets as well as the improved ionic conductivity resulting from the addition of a small amount of LiClO_4 to the PMPyrrBTA-ionic liquid. The areal, volume and specific capacitances of the $\text{MnO}_2@\text{SiNWs}$ symmetric device were derived from the discharging curves measured at different current densities and are plotted in Fig. 6(b,c). Remarkably, the $\text{MnO}_2@\text{SiNWs}$ device exhibits very high areal capacitance with values

up to 13.92 mFcm^{-2} (51 Fg^{-1} , 0.26 Fcm^{-3}) at a current density of 0.4 mAcm^{-2} . These exceptionally good capacitance values can be attributed to the highly porous structure and high specific surface area which facilitate ion transfer and thus enhance redox faradaic reactions and surface adsorption of electrolyte cations. Figure 6(d) compares the areal power and energy densities of the $\text{MnO}_2@/\text{SiNWs}$ device reported in this work to the values reported for other supercapacitors. The as-fabricated $\text{MnO}_2@/\text{SiNWs}$ symmetric device features a maximum areal energy density of $9.1 \mu\text{Whcm}^{-2}$ at a current density of 0.4 mAcm^{-2} , which stays in values of $4.02 \mu\text{Whcm}^{-2}$ (0.07 mWhcm^{-3}) at 1 mAcm^{-2} , again confirming the excellent rate performance of the $\text{MnO}_2@/\text{SiNWs}$ hybrid device as shown in Fig. 6(d). Moreover, the obtained maximum volumetric energy density (0.17 mWhcm^{-3}) is comparable to carbon/ MnO_2 (0.22 mWhcm^{-3} at 0.02 Acm^{-3})³³ whereas the areal energy density is considerably higher than SiNWs and carbon based materials³⁴. For example, CNT/OMC ($1.77 \mu\text{Whcm}^{-2}$, 0.08 mAcm^{-2})³⁵, graphene ($0.17 \mu\text{Whcm}^{-2}$, 0.017 mAcm^{-2})³⁶, plastic wire/ ZnO nanowires on gold films ($0.027 \text{ microWcm}^{-2}$, 2 microampere)³⁷, pen ink ($2.7 \mu\text{Whcm}^{-2}$ ³⁷, 0.083 mAcm^{-2})³⁸, CNT and Ti fibers ($0.15 \mu\text{Whcm}^{-2}$, $0.25 \mu\text{A}$)³⁹, PANI/stainless steel ($0.95 \mu\text{Whcm}^{-2}$, 0.32 mAcm^{-2})⁴⁰. Moreover, Fig. 6(e) shows volumetric power density versus volumetric energy density for the $\text{MnO}_2@/\text{SiNWs}$ sample plotted and compared with other energy storage devices such as electrolytic capacitors and carbon onion micro-supercapacitors⁴¹. It is seen that $\text{MnO}_2@/\text{SiNWs}$ electrode demonstrates relatively higher energy density than conventional capacitors and higher power density than carbon onion micro-supercapacitors. This observation is quite promising in the context of utilizing $\text{MnO}_2@/\text{SiNWs}$ samples for fabricating electrodes in supercapacitor devices.

The electrochemical stability of $\text{MnO}_2@/\text{SiNWs}$ hybrid device was examined by repeated charge-discharge processes at 1 mAcm^{-2} . Figure 6(f), shows the evolution of areal capacitance and capacity retention for 5000 cycles. The areal capacitance decreases from 5.9 to 5.31 mFcm^{-2} after 5000 cycles. The overall capacitance loss for $\text{MnO}_2@/\text{SiNWs}$ device is about 9.1% (90.9% stability) after 5000 cycles. Thus, the unique 3D hierarchical hybrid electrode shows high electrochemical stability for long cycle life applications at high current densities.

Discussion

As described above, hierarchical ultrathin MnO_2 nanoflakes can be controllably grown on SiNWs in order to fabricate $\text{MnO}_2@/\text{SiNWs}$ core-shell hybrid electrodes by a simple solution method followed by a thermal annealing treatment. We would like to discuss here the various reasons why this smartly designed core-shell hetero-structure offers multiple noticeable advantages over previous materials used for micro-supercapacitors applications. For example, (1) well wrapped ultrathin MnO_2 nanoflakes on SiNWs enable a fast, reversible faradaic reaction, and provide a short ion diffusion path. (2) Moreover, a unique 3D mesoporous structure of MnO_2 on SiNWs provides a large-area contact for the electrode and electrolyte and enables accommodation of the large volume change and release of the associated strain generated during rapid charge and discharge cycling. (3) Electrically conducting slim SiNWs directly grown on Si wafer serve both as the backbone and electron superhighway for charge storage and delivery. (4) $\text{MnO}_2@/\text{SiNWs}$ core-shell hetero-structure are strongly supported on Si wafer, avoiding the use of polymer binder/conductive additives and ensuring a sufficiently porous structure, and consequently the “inactive” surface is significantly reduced. (5) Last but not least, The Li^+ doped ionic liquid used here offers additional advantages. Thus, the ionic liquid electrolytes provide a high operating potential of the electrode of 2.2 V whereas LiClO_4 as the primary ionic working species is reversibly inserted into and out of lattice tunnels between the $[\text{MnO}_6]$ octahedral subunits and cause a large amount of a large amount of the manganese oxide to take part in surface redox reactions.

To conclude, we have developed a facile and cost-effective method to grow hierarchical ultrathin MnO_2 nanoflakes on SiNWs in order to fabricate $\text{MnO}_2@/\text{SiNWs}$ hybrid nanocomposite electrodes and demonstrate improved electrochemical performance with Li-ion doped PMPyrrBTA ionic liquid for micro-supercapacitors. By taking advantage of the hybridization of MnO_2 ultrathin nanoflakes and silicon nanowires (SiNWs), we demonstrate that the device fabricated by the $\text{MnO}_2@/\text{SiNWs}$ electrodes can be cycled reversibly at a high operating voltage of 2.2 V and exhibits highest areal capacitance of 13 mFcm^{-2} . The maximum energy density of $9.1 \mu\text{Whcm}^{-2}$ (0.17 mWhcm^{-3}) and maximum power density of $388 \mu\text{Wcm}^{-2}$ (16 mWcm^{-3}) obtained from symmetrical $\text{MnO}_2@/\text{SiNWs}$ devices with a LiClO_4 -PMPyrrBTA IL electrolyte constitute record-breaking values compared with areal energy and power densities reported in the literature for other micro-supercapacitors. Moreover, it exhibits excellent cycling performance with 91% retention after 5000 cycles. This exciting capacitive behavior is attributed to the unique hierarchical $\text{MnO}_2@/\text{SiNWs}$ core-shell hybrid structure coupled with Li ion doped IL liquid. This novel double-hybrid approach (with hybridization at the electrode and the electrolyte) has led to the recent filing of a patent⁴³ and suddenly adds a novel practical route for the elegant design of high-performance micro-supercapacitors.

Method

Fabrication of SiNWs on silicon wafer. Silicon nanowires were fabricated by following the procedure reported elsewhere⁴². SiNWs electrodes with a length of approximately $50 \mu\text{m}$ and a diameter of 50 nm were grown in a CVD reactor (EasyTube3000 First Nano, a Division of CVD Equipment Corporation) by using the vapor-liquid-solid (VLS) method via gold catalysis on highly doped n-Si (111) substrate. Gold colloids with size of 50 nm were used as catalysts, H_2 as carrier gas, silane (SiH_4)

as silicon precursor, phosphine (PH_3) as n-doping gas and HCl as additive gas. The use of HCl has been proven to reduce the gold surface migration and improve the morphology of SiNWs. Prior to the growth, wafer surface was cleaned by successive dipping in acetone, isopropanol and Caro ($\text{H}_2\text{SO}_4\text{-H}_2\text{O}_2$, 3:1 v/v) solutions in order to remove organic impurities, after that, the substrates were dipped in HF 10% and NH_4F solution to remove the native oxide layer. Finally, the gold catalyst was deposited on the surface. The deposition was carried out using HF 10% from an aqueous gold colloid solution. The growth was performed at 600°C , under 6 Torr total pressure, with 40 sccm (standard cubic centimeters) of SiH_4 , 100 sccm of PH_3 gas (0.2% PH_3 in H_2), 100 sccm of HCl gas and 700 sccm of H_2 as supporting gas. The doping level (dl) of the SiNWs was managed by the pressure ratio: dopant gas/ SiH_4 , which was evaluated in previous works (dl: $4 \times 10^{19} \text{ cm}^{-3}$).

Growth of ultrathin MnO_2 nanoflakes on SiNWs. Growth of ultrathin MnO_2 nanoflakes on SiNWs was carried out by a simple chemical bath deposition (CBD) method. Briefly, 2 millimoles KMnO_4 was dissolved in 50 ml of deionized water and then 2 ml of hydrochloric acid (98 wt%) was slowly dropped into the above solution. The solution was transparent and free from any precipitate. Then, silicon wafer with pre-deposited SiNWs was immersed in the bath at a temperature of 323 K. After a few minutes, the solution became blurred and a brown precipitate was formed in the bath. During the precipitation an heterogeneous reaction occurred and the deposition of MnO_2 took place on SiNWs. In order to get uniform coating of MnO_2 , different time intervals such as 5, 10, 15 and 20 min were tested. Finally, MnO_2 @SiNWs substrates were removed, rinsed, and dried in vacuum at 373 K for 2 h.

Characterization techniques. The surface morphology was studied by scanning electron microscopy (FEI Quanta 650 F Environmental SEM). TEM images were obtained with a field emission gun transmission electron microscope (Tecnai G2 F20 S-TWIN HR(S) TEM, FEI). Crystallographic study was carried out using Panalytical X'pert Pro-MRD instrument (Cu K_α radiation and PIXel detector). The X-ray photoelectron spectra (XPS) data were obtained by X-ray photoelectron spectroscopy (XPS, SPECS Germany, PHOIBOS 150). N_2 adsorption/desorption was determined by Brunauer-Emmett-Teller (BET) measurements using Micromeritics instrument (Data Master V4.00Q, Serial#:2000/2400). Electrochemical characterization of MnO_2 @SiNW hybrid electrodes were carried out in 2-electrode configuration with Biologic VMP3 potentiostat. All samples were measured in the typical two-electrode coin cells with MnO_2 @SiNW hybrid ($1 \text{ cm} \times 1 \text{ cm}$) used as both the cathode and anode electrodes. The two electrodes were sandwiched by a PVDF separator and assembled into a coin cell. The material's mass loading on the sponge is obtained by measuring the weight difference before and after MnO_2 deposition by using a microbalance. The electrolytes used in this study include 0.1 M of LiClO_4 /propylene carbonate, 1-Methyl-1-propylpyrrolidinium bis(trifluoromethylsulfonyl)imide (PMPyrrBTA) (purchased from IOLITEC (Ionic Liquids Technologies GmbH, Germany) and 0.01 M LiClO_4 doped ionic liquid electrolyte (LiClO_4 -PMPyrrBTA). All cells were assembled and sealed in an Argon-filled glove box.

References

- Sung, J. H., Kim, S. J., Jeong, S. H., Kim, E. H. & Lee, K. H. Flexible microsupercapacitors. *J. Power Sources* **162**, 1467–1470 (2006).
- Chmiola, J., Largeot, C., Taberna, P. L., Simon, P. & Gogotsi, Y. Monolithic carbide-derived carbon films for micro-supercapacitors. *Science* **328**, 480–483 (2010).
- Pech, D. *et al.* Ultrahigh-power micrometer-sized supercapacitors based on onion-like carbon. *Nat. Nanotech.* **5**, 651–654 (2010).
- Gao, W. *et al.* Direct laser writing of micro-supercapacitors on hydrated graphite oxide films. *Nat. Nanotech.* **6**, 496–500 (2011).
- Adriaanse, C. Microsupercapacitors plugging electronics into T-shirts. *Chem. Ind.* 11–11 (2011).
- Rolison, D. R. *et al.* Multifunctional 3D nanoarchitectures for energy storage and conversion. *Chem. Soc. Rev.* **38**, 226–252 (2009).
- Beidaghi, M. & Wang, C. L. Recent advances in design and fabrication of on-chip micro-supercapacitors. *Proc. SPIE* **8377**, 837708 (2012).
- Pech, D. *et al.* Elaboration of a microstructured inkjet-printed carbon electrochemical capacitor. *J. Power Sources* **195**, 1266–1269 (2010).
- Beidaghi, M. & Wang, C. L. Micro-supercapacitors based on interdigital electrodes of reduced graphene oxide and carbon nanotube composites with ultra-high power handling performance. *Adv. Funct. Mater.* **22**, 4501–4510 (2012).
- Aradilla, D. *et al.* High performance of symmetric micro-supercapacitors based on silicon nanowires using N-methyl-N-propylpyrrolidinium bis(trifluoromethylsulfonyl)imide as electrolyte. *Nano Energy*, **9**, 273–281 (2014).
- Thissandier, F., Pauc, N., Brousse, T., Gentile, P. & Sadki, S. Micro-ultracapacitors with highly doped silicon nanowires electrodes. *Nanoscale Res. Lett.* **8**, 38 (2013).
- Berton, N. *et al.* Wide-voltage-window silicon nanowire electrodes for micro-supercapacitors via electrochemical surface oxidation in ionic liquid electrolyte. *Electrochem. Commun.*, **41**, 31–34 (2014).
- Alper, J. P., Vincent, M., Carraro, C. & Maboudian, R. Silicon carbide coated silicon nanowires as robust electrode material for aqueous micro-supercapacitor. *Appl. Phys. Lett.*, **100**, 163901 (2012).
- Rowlands, S. E. & Latham, R. J. Supercapacitor devices using porous silicon electrodes. *Ionics*, **5**, 144–149 (1999).
- Desplombain, S., Gautier, G., Semai, J., Ventura, L. & Roy, M. Investigations on porous silicon as electrode material in electrochemical capacitor. *Phys. Stat. Sol. (C)*, **4**, 2180–2184 (2007).
- Tao, B., Zhang, J., Miao, F., Hui, S. & Wan, L. Preparation and electrochemistry of NiO/SiNW nanocomposite electrodes for electrochemical capacitors. *Electrochim. Acta*, **55**, 5258–5262 (2010).
- Lu, F. *et al.* Electrochemical properties of high power supercapacitors using ordered NiO coated Si nanowire arrays electrodes. *Appl. Phys. A*, **104**, 545–550 (2011).

18. Aradilla, D. *et al.* Novel hybrid micro-supercapacitor based on conducting polymer coated silicon nanowires for electrochemical energy storage. *RSC Adv.*, **4**, 26462–26467 (2014).
19. Chang, J. K., Lee, M. T., Tsai, W. T., Deng, M. J. & Sun, I. W. X-ray photoelectron spectroscopy and *in situ* X-ray absorption spectroscopy studies on reversible insertion/desertion of dicyanamide anions into/from manganese oxide in ionic liquid. *Chem. Mater.*, **21**, 2688–2695 (2009).
20. Lee, M. T. *et al.* Pseudocapacitance of MnO₂ originates from reversible insertion/desertion of thiocyanate anions studied using *in situ* X-ray absorption spectroscopy in ionic liquid electrolyte. *J. Power Sources*, **195**, 919–922 (2010).
21. Liu, J. *et al.* Co₃O₄ nanowire@MnO₂ ultrathin nanosheet core/shell arrays: a new class of high-performance pseudocapacitive materials. *Adv. Mater.*, **23**, 2076–2081 (2011).
22. Zhou, J. *et al.* Novel synthesis of birnessite-type MnO₂ nanostructure for water treatment and electrochemical capacitor. *Ind. Eng. Chem. Res.* **52**, 9586–9593 (2013).
23. Xia, H. *et al.* Hierarchically structured Co₃O₄@Pt@MnO₂ nanowire arrays for high-performance supercapacitors. *Sci. Rep.* **3**, 2978 (2013).
24. Huang, M. *et al.* Merging of Kirkendall growth and Ostwald ripening: CuO@MnO₂ core-shell architectures for asymmetric supercapacitors. *Sci. Rep.* **4**, 4518 (2014).
25. Wei, W., Cui, X., Chen, W. & Ivey, D. G. Manganese oxide-based materials as electrochemical supercapacitor electrodes. *Chem. Soc. Rev.*, **40**, 1697–1721 (2011).
26. Dubal, D. P., Kim, J. G., Kim, Y., Holze, R. & Kim, W. B. Demonstrating the highest supercapacitive performance of branched MnO₂ nanorods grown directly on flexible substrates using controlled chemistry at ambient temperature. *Energy Technol.* **1**, 125–130 (2013).
27. Dubal, D. P., Gund, G. S., Holze, R. & Lokhande, C. D. Mild chemical strategy to grow micro-roses and micro-woolen like arranged CuO nanosheets for high performance supercapacitors. *J. Power Sources*, **242**, 687–698 (2013).
28. Wang, Y. *et al.* Printed all-solid flexible microsupercapacitors: towards the general route for high energy storage devices. *Nanotechnol.* **25**, 094010 (2014).
29. Li, L., Chen, C., Xie, J., Shao, Z. & Yang, F. The preparation of carbon nanotube/MnO₂ composite fiber and its application to flexible micro-supercapacitor. *J. Nanomater.* **2013**, 1–5 (2013).
30. Ren, J. *et al.* Twisting carbon nanotube fibers for both wire-shaped micro-supercapacitor and micro-battery. *Adv. Mater.*, **25**, 1155–1159 (2013).
31. Huang, P. *et al.* Micro-supercapacitors from carbide derived carbon (CDC) films on silicon chips. *J. Power Sources*, **225**, 240–244 (2013).
32. Huang, P. *et al.* On-chip micro-supercapacitors for operation in a wide temperature range. *Electrochem. Commun.*, **36**, 53–56 (2013).
33. Xiao, X. *et al.* Fiber-based all-solid-state flexible supercapacitors for self-powered systems. *ACS Nano*, **6**, 9200–9206 (2012).
34. Le, V. T. *et al.* Coaxial fiber supercapacitor using all-carbon material electrodes. *ACS Nano*, **7**, 5940–5947 (2013).
35. Ren, J., Bai, W., Guan, G., Zhang, Y. & Peng, H. Flexible and weavable capacitor wire based on a carbon nanocomposite fiber. *Adv. Mater.*, **25**, 5965–5970 (2013).
36. Meng, Y. *et al.* All-graphene core-sheath microfibers for all-solid-state stretchable fibriform supercapacitors and wearable electronic textiles. *Adv. Mater.*, **25**, 2326–2331 (2013).
37. Bae, J. *et al.* Fiber supercapacitors made of nanowire-fiber hybrid structures for wearable/flexible energy storage. *Angew. Chem. Int. Ed.*, **50**, 1683–1687 (2011).
38. Fu, Y. *et al.* Fiber supercapacitors utilizing pen ink for flexible/wearable energy storage. *Adv. Mater.*, **24**, 5713–5718 (2012).
39. Chen, T. *et al.* An integrated ‘energy wire’ for both photoelectric conversion and energy storage. *Angew. Chem. Int. Ed.*, **41**, 11977–11980 (2012).
40. Fu, Y. *et al.* Integrated power fiber for energy conversion and storage. *Energy Environ. Sci.*, **6**, 805–812 (2013).
41. Xiong, G., Meng, C., Reifenger, R. G., Irazoqui, P. P. & Fisher, T. S. A review of graphene-based electrochemical microsupercapacitors. *Electroanalysis*, **26**, 30–51 (2014).
42. Gentile, P. *et al.* Effect of HCl on the doping and shape control of silicon nanowires. *Nanotechnology*, **23**, 215702 (2012).
43. Dubal, D. P. *et al.* European Patent EU15158311 March 9, 2015. Electrode Material Comprising Silicon Nanowires Covered By Mesoporous Oxide Nanostructured Coating And Ionic Liquid Electrolytes For Energy Storage Applications.

Acknowledgments

The authors acknowledge the financial support from the European Commission’s Seventh Framework Program for Research, Technological Development and Demonstration under Grant agreement no.309143 (NEST, 2012-2015). ICN2 acknowledges support of the Spanish MINECO through the Severo Ochoa Centers of Excellence Program under Grant SEV-2013-0295. Authors appreciate the award to DPD of a Marie-Curie Fellowship through Beatriz de Pinos Program (BP-DGR-2013) for Catalan system of science and technology, Spain.

Author Contributions

D.P.D. and P.G.R. designed the experiments, analyzed the data and wrote the manuscript. D.A., G.B., P.G. and S.S. carried out synthesis and characterization of silicon nanowires. T.J.S.S. and J.W. provide the ionic liquids. D.P.D. and P.G.R. designed and carried out synthesis and electrochemical measurements of hybrid thin films. To the preparation and reviewing manuscript, all authors contributed equally.

Additional Information

Supplementary information accompanies this paper at <http://www.nature.com/srep>

Competing financial interests: The authors declare no competing financial interests.

How to cite this article: Dubal, D. P. *et al.* 3D hierarchical assembly of ultrathin MnO₂ nanoflakes on silicon nanowires for high performance micro-supercapacitors in Li- doped ionic liquid. *Sci. Rep.* **5**, 9771; doi: 10.1038/srep09771 (2015).



This work is licensed under a Creative Commons Attribution 4.0 International License. The images or other third party material in this article are included in the article’s Creative

Commons license, unless indicated otherwise in the credit line; if the material is not included under the Creative Commons license, users will need to obtain permission from the license holder to reproduce the material. To view a copy of this license, visit <http://creativecommons.org/licenses/by/4.0/>